Wet chemical synthesis of self-standing single-crystalline copper telluride Cu7Te4 nanorods: Characterizations and mechanism

K Al Hokayem, L M Adam, J Ghanbaja, Abdelkrim Redjaïmia, E Haye, S Michel, S Legeai, N Stein

Materials Chemistry and Physics 318 (2024) 129239

Contents lists available at ScienceDirect

Materials Chemistry and Physics

journal homepage: www.elsevier.com/locate/matchemphys

Wet chemical synthesis of self-standing single-crystalline copper telluride Cu_7Te_4 nanorods: Characterizations and mechanism

K. Al Hokayem [a], L.M. Adam [a,*], J. Ghanbaja [b], A. Redjaïmia [b], E. Haye [c], S. Michel [a], S. Legeai [a], N. Stein [a,**]

[a] Université de Lorraine, CNRS, IJL, F-57000, Metz, France
[b] Université de Lorraine CNRS, IJL, F-54000, Nancy, France
[c] Laboratoire d'Analyse par Réactions Nucléaires (LARN), Namur Institute of Structured Matter (NISM), University of Namur, 5000, Namur, Belgium

HIGHLIGHTS

- Synthesis of single crystalline Cu_7Te_4 nanorods with a homogeneous chemical composition along the nanorods.
- Final step with a soft chemical transformation at room temperature and atmospheric pressure.
- Reaction of disproportionation of Tellurium leading to Cu_7Te_4 proven by thermodynamic calculations.
- Detailed analysis of the microstructure highlighting the presence of stacking local defects.

GRAPHICAL ABSTRACT

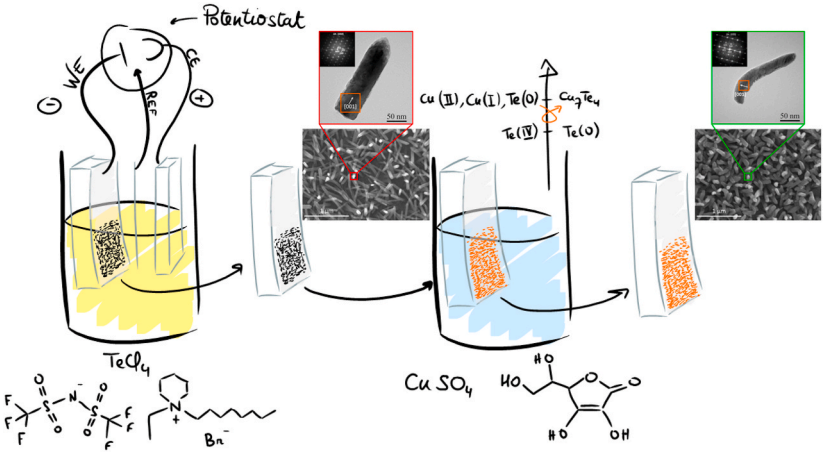

ARTICLE INFO

Keywords:
Copper telluride
Chemical synthesis
Disproportionation
Nanostructure
Single crystalline
Tellurium

ABSTRACT

Single crystalline Cu_7Te_4 nanorods were obtained from a two-step synthesis route. The first step is the electrochemical deposition of self-standing tellurium nanorods on Pt-coated glass electrode in an ionic liquid electrolyte acting as a structuring solvent. Afterwards, soft chemical transformation in Cu_7Te_4 is performed by immersing the Te-covered electrode in a Cu(II) solution in presence of ascorbic acid acting as reducer at room temperature and atmospheric pressure. Tellurium seems to undergo a reaction of disproportionation induced by the simultaneous presence of Cu(II) and Cu(I) into Te(IV) and Cu_7Te_4, which is supported by thermodynamic considerations. The copper telluride nanorods were analyzed by XRD, SEM-EDX, HRTEM-FFT/SAED, EELS and XPS that allowed to set the required parameters in terms of molar ratio of precursors in the bath to induce the targeted chemical reaction. The analyses highlight the obtention of single crystalline Cu_7Te_4 with a homogeneous

* Corresponding author.
** Corresponding author.
E-mail addresses: laura.adam@univ-lorraine.fr, adam.lauramarie@gmail.com (L.M. Adam), nicolas.stein@univ-lorraine.fr (N. Stein).

https://doi.org/10.1016/j.matchemphys.2024.129239
Received 27 October 2023; Received in revised form 11 March 2024; Accepted 23 March 2024

chemical composition along the nanorods. A detailed analysis of the microstructure shows the presence of stacking local defects, leading to curved nanostructures.

1. Introduction

The non-stoichiometric copper telluride $Cu_{2-x}Te$ compounds include a wide range of compositions and phases with varied physical and chemical properties and therefore with multiple applications [1]. Among these phases, there is considerable interest in Cu_7Te_4 as a material for energy. Indeed, this binary compound behaves like a highly degenerate p-type semiconductor [2] and can be considered for thermoelectric conversion [3]. Furthermore, nanostructuring these compounds is of particular interest as they are expected to offer better properties, including larger active surface area and reduced lattice thermal conductivity [4]. Thus, according to Tan et al. [3], the addition of Cu_7Te_4 nanorods to a $Bi_{0.4}Sb_{1.6}Te_3$ matrix results in enhanced thermoelectric properties. Besides, it appears that this particular phase of copper telluride can serve as an effective substitute for the anode material in aqueous Zn-ion batteries [5], the hybrid anode of $Zn@Cu_7Te_4$ inducing a longer cycling time and a better electrochemical behavior than bare Zn [6]. Finally, it should also be noted that Cu_7Te_4 is interesting for its electrocatalytic properties, in particular Cu_7Te_4 nanosheets show superior oxygen evolution reaction (OER) performance and durability than their bulk counterpart in alkaline solution [7].

$Cu_{2-x}Te$ copper tellurides nanostructures can be synthesized by soft chemistry routes such as electrochemical deposition [8–12], solvothermal synthesis [13–18] and hydrothermal synthesis [19–21]. These two latter kind of methods can be assisted by microwave [14] or ultrasound activation [18]. The reaction takes place in an aqueous solution (hydrothermal synthesis) or an organic solvent (solvothermal synthesis) like ethylene glycol (EG) [14], oleic acid [22], tri-*n*-octyl phosphine (TOP) [15], acetone [16], ethylenediamine (EDA) [17–19]. A reducing agent can be added ($NaBH_4$ [14], hydrazine N_2H_4 [20,21,23], ascorbic acid [13,24]) but some organic solvents can also play this role (TOP, EG, EDA).

Whether using a chemical or electrochemical approach, the synthesis can be implemented in one step with co-reduction of Cu and Te precursors [8,11,12,16,19,25,26], or in 2 steps with a first step devoted to the synthesis of Te nanostructures [9,14,23,24]. When the synthesis takes place in 2 steps, the crystallinity of the Te nanostructures can be preserved. For example, Dong et al., using hexagonal 1D Te nanotubes synthesized in a first step, obtained hexagonal single crystal $Cu_{2-x}Te$ nanowires by microwave assisted chemical reduction [14]. Similarly, by 2-steps hydrothermal synthesis at 200 °C, Wan et al. obtained $Cu_{2-x}Te$ hexagonal single-crystal 1D nanowires without stacking or dislocation defects [20].

The reaction mechanism of the formation of copper telluride compounds involved in the 2-steps synthesis route is quite complex and two different mechanisms have been proposed in the literature. A hypothesis involving Cu(I) as an intermediate species is proposed. Cu(I) can be directly introduced as CuCl for example [15] or generated *in situ* by Cu (II) chemical reduction using either hydrazine [20,21,23] or ascorbic acid [13,24]. The presence of Cu(I) then induces a disproportionation reaction of Te(0) nanostructures into Te(-II) and Te(IV) leading to the formation of copper telluride [24]. Another hypothesis is based on a topotactic reaction, where Cu(0), reduced from Cu(II) precursor, is incorporated in the initial Te nanostructures as proposed by Wang et al. [23] and Dong et al. [18].

In this work, we propose an original synthesis method of Cu_7Te_4 nanorods using a two-step reaction scheme. The interest of the developed approach is the experimental protocol based on soft chemistry with ecofriendly reagents and carried out at atmospheric pressure and room temperature. The first step corresponds to the electrodeposition of one-dimensional hexagonal single crystalline Te nanorods in a templating ionic liquid electrolyte, from operating conditions developed in our previous work [27]. In a second step, Te nanorods are immersed in an aqueous solution containing ascorbic acid and Cu(II) ions at room temperature, thus without any addition of toxic solvents, surfactants or complexing agents. The different parameters affecting the progress of this second step are presented. The presence of Cu(I) in the final product is evidenced by experimental means and the mechanism based on Te(0) disproportionation reaction is supported by thermodynamic considerations. The synthesis results in single-crystalline Cu_7Te_4 nanorods, that are self-standing on a Pt substrate.

2. Experimental section

2.1. Chemicals

$TeCl_4$ (99%) used as precursor of Te(IV) was purchased from Alfa Aesar. $CuSO_4$, $5H_2O$ (99.8 %) used as precursor of Cu(II) was purchased from VWR as well as L-ascorbic acid $C_6H_8O_6$ (99 %). 1-ethyl-1-octyl-piperidinium bromide (EOPipBr) and 1-ethyl-1-octyl-piperidinium bis (trifluoromethylsulfonyl)imide (EOPipTFSI) ionic liquids (ILs) were synthesized as described by Traore et al. [28]. These ILs were stored in a glove box to minimize water/oxygen contents (Mbraun Labstar, O_2/H_2O levels <1 ppm).

2.2. Synthesis of Cu_7Te_4 nanostructures

First step: Single crystalline Te nanorods, with homogeneous dimensions, were obtained by potentiostatic electrodeposition with a coulombic charge density of $0.1C{\cdot}cm^{-2}$ [27]. The deposition potential is determined by a linear sweep voltammetry prior to the deposition. The solution was composed of 5 $mmol{\cdot}L^{-1}$ $TeCl_4$ dissolved in a mix of two ILs EOPipTFSI:EOPipBr 95:5 mol% as electrolyte. This first step took place at 100 °C in a glove box. These conditions are of primary importance for the synthesis of single crystalline Te nanostructures in this viscous and hygroscopic ionic liquid medium. EOPipBr improves the solubility of $TeCl_4$ in EOPipTFSI since bromide anion acts as a complexing agent for Te(IV). EOPipTFSI has templating properties and allows to synthesize one-dimensional nanostructures [29–31]. The major advantage of this synthesis method is to avoid the use of porous membrane and additional post-treatment steps such as membrane dissolution, nanostructures cleaning and dispersion [32]. Moreover, after the synthesis, the nanostructures are self-standing on the substrate and can be easily handled and modified by electrochemical or chemical treatment [33].

The electrodeposition and the voltammetry were performed in a three-electrodes cell containing 5 mL of deposition solution, using a Biologic VMP300 potentiostat. A Pt wire was used as a pseudo-reference electrode. 300 nm thick Pt-coated glass slides (25 × 10 × 1 mm) purchased from Applications Couches Minces (ACM) were used as working and counter electrodes. These two electrodes were cleaned from organic contamination before Te deposition by sonication in acetone (2 × 20 min), in ethanol (20 min) and then air-dried. Afterwards, the cleaned Pt surface of the working electrode was chemically activated by immersion in 7 $mol{\cdot}L^{-1}$ HNO_3 and electrochemically activated by cyclic voltammetry in 0.5 $mol{\cdot}L^{-1}$ H_2SO_4 (50 scans between −0.17 V vs Ag/AgCl and 1.2 V vs Ag/AgCl) to promote a uniform growth of Te nanorods.

The deposition surfaces were delimited by a piece of Kapton adhesive and equal to 0.5 cm^2. The applied potential for Te electrodeposition was equal to the potential of the reduction peak corresponding to Eq. (1), determined before each deposition by linear sweep voltammetry under natural diffusion conditions [31]:

Table 1
Solutions compositions used for chemical transformations.

Bath	Comment	$[Cu^{2+}]$ (mol·L^{-1})	$[C_6H_8O_6]$ (mol·L^{-1})	$n_{Te}^{theoretical}$ (mol)	Molar ratio $C_6H_8O_6$/Cu	Molar ratio Cu/Te
A	Cu large excess/$C_6H_8O_6$ excess	$1.0{\cdot}10^{-2}$	$2.0{\cdot}10^{-2}$	$1.3{\cdot}10^{-7}$	2	772
B	Cu large excess/$C_6H_8O_6$ stoichiometry	$1.0{\cdot}10^{-2}$	$5.0{\cdot}10^{-3}$	$1.3{\cdot}10^{-7}$	0.5	772
C	Cu excess/$C_6H_8O_6$ stoichiometry	$5.2{\cdot}10^{-3}$	$2.6{\cdot}10^{-3}$	$1.3{\cdot}10^{-7}$	0.5	400
D	Cu near stoichiometry/$C_6H_8O_6$ stoichiometry	$2.6{\cdot}10^{-5}$	$1.3{\cdot}10^{-5}$	$1.3{\cdot}10^{-7}$	0.5	2

$$TeX_6^{2-} + 4e^- \rightarrow Te + 6X^- \; ; X = Br^- \; or \; Cl^- \qquad \text{Eq. 1}$$

Second step: As-deposited Te nanorods were converted into Cu_7Te_4 nanorods by impregnation. The Te nanorods supported by Pt electrode were immersed in 10 mL of a $CuSO_4$ aqueous solution, under magnetic stirring and at room temperature. Ascorbic acid $C_6H_8O_6$ was added as a reducing agent according Eq. (2).

$$2\,Cu(II) + C_6H_8O_6 \rightarrow 2\,Cu(I) + C_6H_6O_6 + 2\,H^+ \qquad \text{Eq. 2}$$

The influence of Cu(II):Te molar ratio as well as $C_6H_8O_6$:Cu(II) molar ratio and conversion reaction time on the final composition of Cu_7Te_4 nanorods were studied. Four solutions referenced as A, B, C and D were prepared and their composition are summarized in Table 1. The Cu(II): Te molar ratio was varied from a very large Cu excess to a value close to Cu_7Te_4 stoichiometry. $C_6H_8O_6$ was introduced whether in excess or in stoichiometric proportion according to Eq. (2) ($C_6H_8O_6$:Cu(II) = 0.5). The amount of substance of Te ($n_{Te}^{Theoretical}$) electrodeposited on Pt substrate was determined using the Faradaic law (Eq. (3))

$$n_{Te}^{Theoretical} = \frac{Q \times A}{n_{e^-} \times F} \qquad \text{Eq. 3}$$

With: Q, the charge density (C·cm^{-2}); A, the electroactive surface (cm^2); n_{e^-}, the number of electrons exchanged according to Eq. (1); F, the Faradaic constant, 96,484 C·mol^{-1}.

2.3. Characterizations of the nanorods

Scanning Electron Microscopy (SEM) was performed on Zeiss Gemini 500 microscope equipped with an Energy Dispersive X-ray (EDX) detector to analyze the morphology and chemical composition of Te and Cu_7Te_4 nanostructured films.

The faradic yield of Te electrodeposition step and the chemical composition of Cu_7Te_4 nanorods were determined by Inductively Coupled Plasma-Optical Emission Spectrometry (ICP-OES) using a PerkinElmer Avio 200-OES, after the dissolution of the deposits in a 7 mol·L^{-1} HNO_3. Signals were collected through a cooled CCD-based detector, with simultaneous measurement of the background emission and a neon spectrum for active wavelength correction. The ICP-OES instrument was furnished with a slot quartz torch, an alumina 2 mm injector, a cyclonic chamber and a Meinhardt k1 nebulizer. The operating parameters were as follow: RF power: 1.5 kW; plasma gas flow 10 L·min^{-1}, auxiliary gas flow 0.2 L·min^{-1}, nebulizer gas flow 0.7 L·min^{-1} and sample uptake rate 1.0 L·min^{-1}. The following atomic line wavelengths were used in the measurements: Cu (327.393 nm) and Te (214.281 nm). Analysis were triplicate and the distribution were calculated through the standard error and student's t value for a 95% probability.

X-Ray Diffraction (XRD) patterns were obtained using a Bruker D8 Advance diffractometer with Cu Kα radiation (λ = 1.5406 Å) at 40 kV and 40 mA. The scanning range in the 2θ Bragg angle was from 20° to 60°, where all the main peaks of the Te and copper telluride phases were expected. The crystallographic phases were analyzed on the basis of the JCPDS databases with the EVA 5 software®.

High Resolution Transmission Electron Microscopy (HRTEM) investigations were performed on a JEM-ARM 200F Cold Field Emission Gun TEM/Scanning TEM (CFEG TEM/STEM) operating at 200 kV and equipped with a spherical aberration (Cs) probe and image correctors (point resolution 0.12 nm in TEM mode and 0.078 nm in STEM mode). The mean diameter and length of Te and Cu_7Te_4 nanorods were measured on images of individual objects by this instrument. The crystal structure of the nanostructures was analyzed by electron diffraction (SAED; Selected Area Electron Diffraction) and HRTEM images (FFT; Fast Fourier Transformation). The chemical composition of individual nanostructures was determined by EDX (mapping and line profile). The oxidation state of copper was estimated using Electron Energy Loss Spectroscopy (EELS). The chemistry of the sample has been further investigated by X-ray photoelectron spectroscopy (XPS) performed on a Thermo ESCALAB 250Xi spectrometer, working with excitation source Al Kα 1486.68 eV, with a spot size of 250 × 250 μm^2. The sample have been cleaned by cluster gun (500, 6 keV, raster size 1.25 × 1.25 mm). Then, the C1s, O1s, Cu2p and Te3d levels (including Cu LMM) have been acquired with a pass energy of 20 eV, with 20 scans. A flood gun has been used for charge compensation and no further charge shift has been used. The eventual charge shift has been checked on the position of the valence band spectra. The authors are aware of the recent warnings about the charge shift problem and the careful attention needed on the data analysis [34–36].

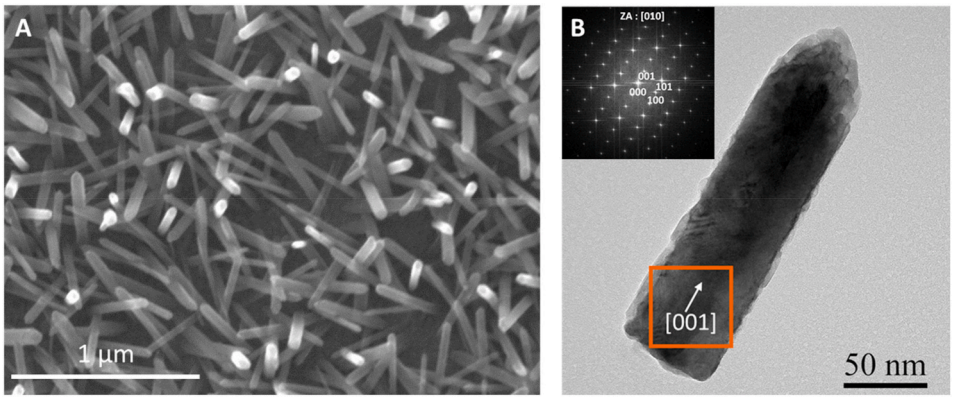

Fig. 1. SEM (A) and TEM (B) micrographs (FFT in inset) of Te nanorods electrodeposited in EOPipTFSI:EOPipBr 95:5 (mol%). $[TeCl_4]$ = 5 mmol·L^{-1}. T = 100 °C, Q = 0.1C·cm^{-2}.

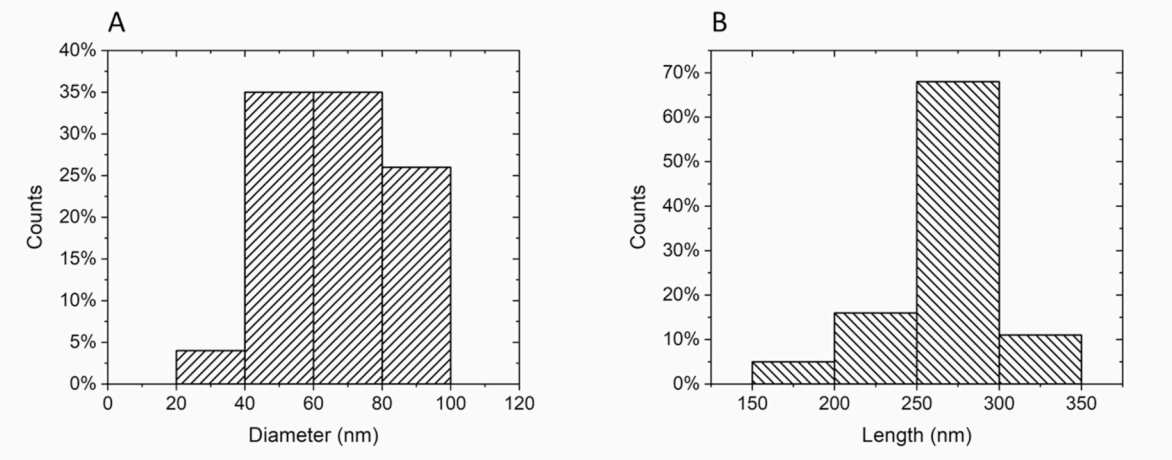

Fig. 2. a) Diameter (n = 20 analyzed nanowires) and b) Length (n = 18 analyzed nanowires) of Te nanorods composing the deposit presented in Fig. 1.

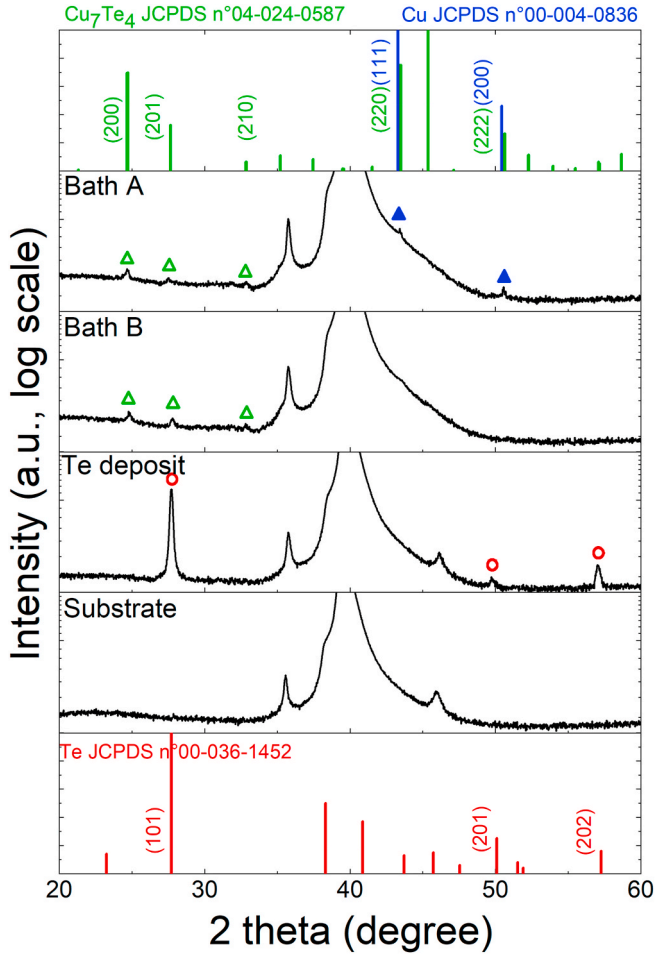

Fig. 3. XRD characterizations to study the influence of molar ratio $C_6H_8O_6$/Cu (II) after 2 h immersion in bath A (Cu large excess/$C_6H_8O_6$ excess) and in bath B (Cu large excess/$C_6H_8O_6$ stoichiometry) on the crystallographic transition from trigonal Te to trigonal Cu_7Te_4, using, for convenience, hexagonal unit cells. Peaks related to Cu_7Te_4, Cu and Te are represented by green triangles, blue triangles and red circles, respectively. The broad peaks at 36° and 40° are related to the substrate. (For interpretation of the references to colour in this figure legend, the reader is referred to the Web version of this article.)

3. Results and discussion

First step: SEM and TEM micrographs of typical single crystalline Te electrodeposit obtained in the experimental conditions detailed in our previous work are presented in Fig. 1 [27]. The deposits are composed of self-standing tellurium nanorods of homogeneous and reproducible dimensions, typically with an average diameter of 52 ± 11 nm and an average length of 237 ± 33 nm (Fig. 2). The nanorods adopt a hexagonal base and end in needle shape. The electrochemical growth is faster in the center part than in the external part leading to tip-shaped as already observed in the literature [32,37]. This tip effect can be due to higher current density at the center of the nanorods. This hexagonal prismatic shape has to be connected to the crystallographic structure.

The Te nanorods are monocrystalline, which crystallize in the primitive trigonal Bravais lattice and belong to the space groups $P3_121$. For convenience, a hexagonal unit cell is adopted with the following lattice parameters a = 4.46 Å et c = 5.92 Å (JCPDS n° 00-036-1452). The TEM analysis reveals that these nanorods exhibit a preferential orientation along the [001] direction. Microstructural analysis and growth mechanism of this first step are detailed in previous works [27,29,30]. The mass per unit area of electrodeposited Te nanorods on activated Pt surfaces is equal to 30 μg/cm^2, corresponding to a faradic yield of 90%.

Second step: Cu_7Te_4 nanorods.

The electrodes with pre-deposited tellurium nanorods were immersed into 10 mL of an aqueous solution containing Cu(II) and ascorbic acid to convert Te to Cu_7Te_4. The specific role of ascorbic acid is to reduce Cu(II) to Cu(I). A first attempt was realized according to the experimental conditions of Zhou et al. [13], namely [Cu(II)] = 10 mmol·L^{-1} and [$C_6H_8O_6$] = 20 mmol·L^{-1}. In this electrolyte solution (bath A, Table 1), according to the amount of deposited Te, Cu(II) is in large excess regarding Te, namely n(Cu(II))/n(Te) = 772, and the n($C_6H_8O_6$)/n(Cu(II)) ratio is equal to 2. It must be mentioned here that, to the authors' knowledge, no indication of the n(Cu(II))/n(Te) ratio is ever given in the related literature.

In order to determine if Cu(I) is involved in the formation of copper telluride, the ratio n($C_6H_8O_6$)/n(Cu(II)) = 0.5 was also studied, by adjusting the $C_6H_8O_6$ concentration to 5 mmol·L^{-1} and thus keeping the same ratio n(Cu(II))/n(Te) = 772 (bath B, Table 1). The molar ratio ($C_6H_8O_6$)/(Cu(II)) equal to 0.5 corresponds to the stoichiometric proportions of the reduction of Cu(II) into Cu(I) according to Eq. (2).

XRD analyses of the nanostructured films (Fig. 3) were first carried out to get initial information on the result of the chemical transformation. After 2 h of reaction and whatever the n($C_6H_8O_6$)/n(Cu(II)) ratio, namely for the baths A and B, the diffraction peaks corresponding to Te disappear completely which confirm the total conversion of Te, while small diffraction peaks appear. By considering the additional

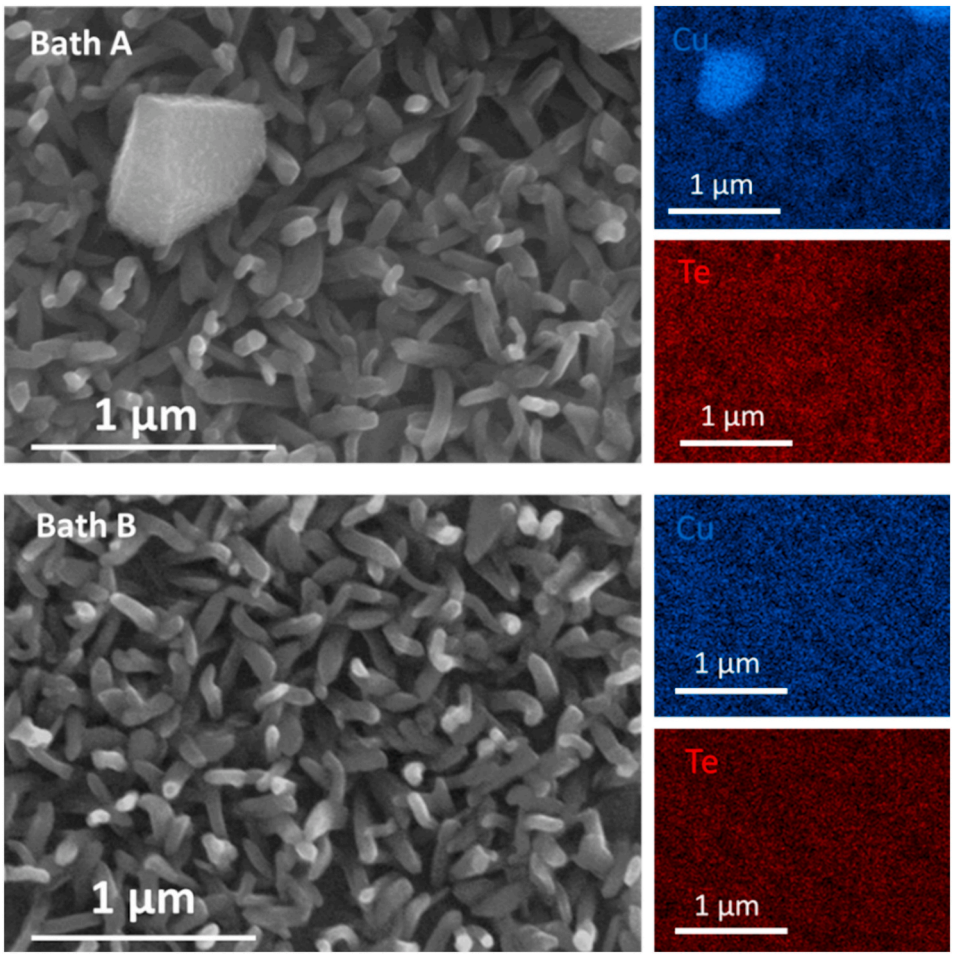

Fig. 4. SEM characterizations and corresponding EDX mapping of Cu_7Te_4 nanorods film after 2 h immersion in bath A (Cu large excess/$C_6H_8O_6$ excess) and in bath B (Cu large excess/$C_6H_8O_6$ stoichiometry).

characterizations hereafter (ICP-OES, SEM-EDX, STEM-EDX, SAED, FFT, XPS), some of these additional peaks, located at 24.6°, 27.5° and 32.9°, can be assigned to the Cu_7Te_4 phase which crystallizes in the primitive trigonal Bravais lattice and belongs to the space group $P\bar{3}m1$ (164). The lattice parameters of the corresponding hexagonal lattice are: a = 8.318 Å and c = 7.223 Å [38]. Note that two additional peaks at 43.3° and 50.5° appear only for bath A. Although they may coincide with the (220) and (222) Cu_7Te_4 diffraction planes respectively, the attribution to the (111) and (200) copper diffraction planes seems more relevant in view of analysis below (EDX mapping and ICP-OES).

When $n(C_6H_8O_6)/n(Cu(II)) = 2$ (bath A), SEM-EDX analysis of the surfaces after conversion (Fig. 4) reveals the additional presence of large Cu(0) particles on the surface of the nanorods film. Orange particles (Cu (0)) in suspension were also observed in the solution. On the contrary, when the ratio $n(C_6H_8O_6)/n(Cu(II))$ is equal to 0.5 (bath B), no Cu(0) particles were observed on the deposit and the solution remains clear. From these observations, we can deduce that if ascorbic acid is introduced in excess with respect to Eq. (2) ($n(C_6H_8O_6)/n(Cu(II)) = 2$, bath A), Cu(II) is partially reduced down to Cu(0) according to Eq. (4). These observations are consistent with the mechanism in which Cu_7Te_4 formation would imply Cu(II) reduction into Cu(I).

$$Cu(II) + C_6H_8O_6 \rightarrow Cu(0) + C_6H_6O_6 + 2H^+ \quad \text{Eq. 4}$$

In a complementary way, we placed commercial Te particles of dimensions from 80 to 100 nm (Nanoshell) in an aqueous solution of ascorbic acid (2 mol·L^{-1}), this experiment does not lead to any change on the tellurium particles, proving that ascorbic acid does not reduce Te (0) into Te(-II). The formation of Cu_7Te_4 then probably implies a disproportionation reaction of Te(0) in the presence of Cu(I), as claimed by Zhou et al. [13] and Park et al. [24]. This hypothesis is discussed from a thermodynamic point of view later in this paper.

An additional analysis, the ICP-OES measurement resulting from the dissolution in 7 mol·L^{-1} HNO_3 of the transformed nanorods, shows that the atomic percentage of copper in the deposits, at.% (Cu), is higher when $C_6H_8O_6$ is in excess (bath A) in the conversion bath. When the molar ratio $(C_6H_8O_6)/(Cu(II))$ is equal to 0.5 (bath B), the chemical content of the deposit exhibits at.%(Cu) = 62.80% ± 0.03% (N = 3; 95%) in agreement with the Cu_7Te_4 stoichiometry (theoretical at.%(Cu) = 63.6 %). However when $n(C_6H_8O_6)/n(Cu(II)) = 2$ (bath A), an excess of copper is observed (at.%(Cu) = 84.2 % ± 0.3%; N = 3; 95%), which is attributed to the additional presence of Cu(0) particles.

In the two experimental sets of conditions, the nanorods are curved after their transformation and the appearance of the surface changes at the edges when compared to Te nanorods (Fig. 1). On the other hand, there is no significant increase of their dimensions. The EDX analysis (Fig. 4) highlights the homogeneity of the composition of the films in the case of $n(C_6H_8O_6)/n(Cu(II)) = 0.5$ (bath B) as well as in the case of excess of ascorbic acid ($n(C_6H_8O_6)/n(Cu(II)) = 2$; bath A) with the exception of the large Cu(0) particles present on the surface. STEM-EDX analysis of a single nanorod obtained with the optimal ratio $n(C_6H_8O_6)/n(Cu(II)) = 0.5$ is shown in Fig. 5. The composition is homogeneous along the diameter with the exception of two extreme edge points. The chemical conversion of Te into Cu_7Te_4 is confirmed as proven by the average copper atomic ratio at.%(Cu) = 64%.

The HRTEM micrograph and corresponding FFT confirm that the

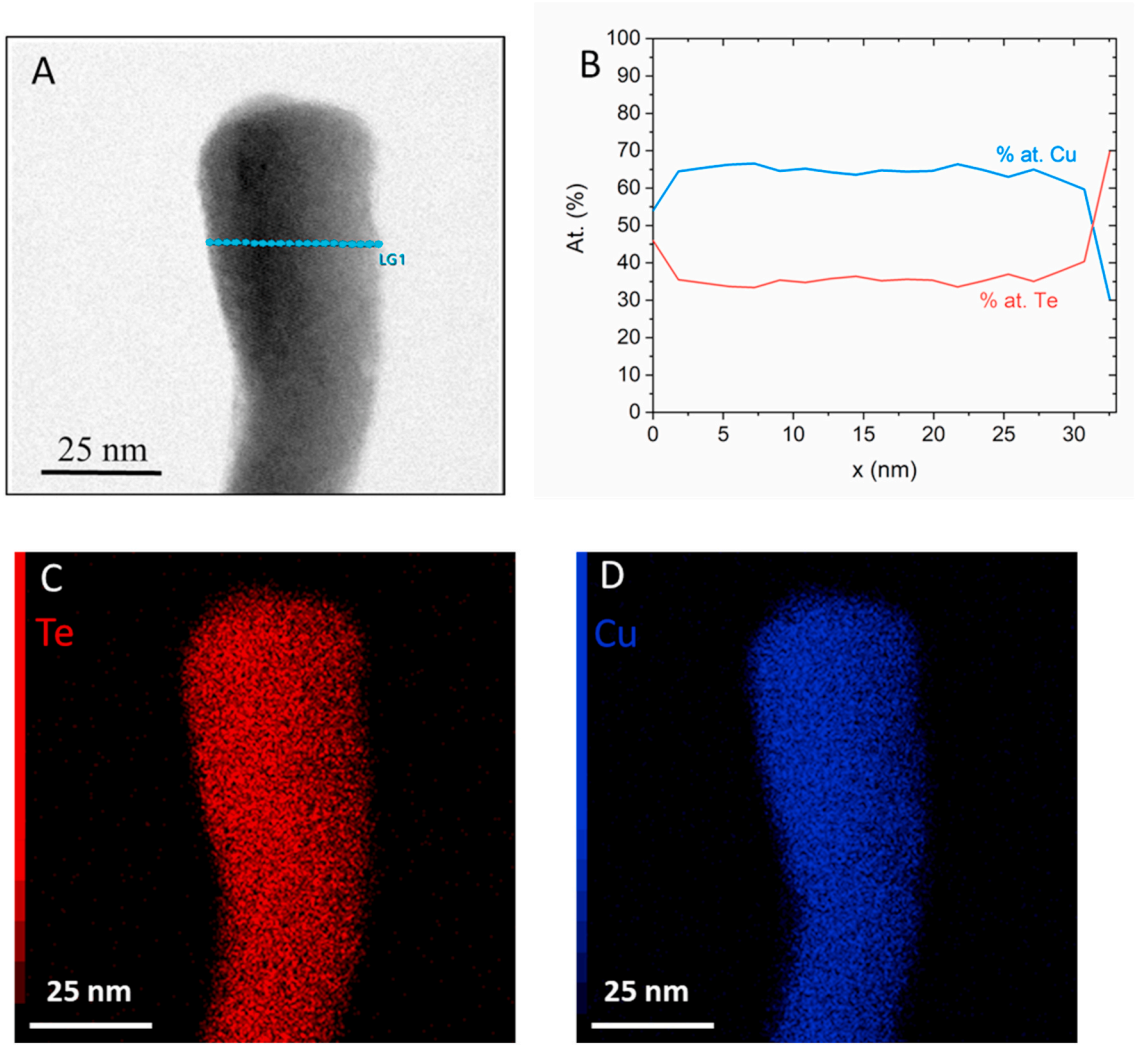

Fig. 5. STEM-EDX characterizations of a Cu_7Te_4 nanorod after 2 h immersion in bath B (Cu large excess/$C_6H_8O_6$ stoichiometry) (A). EDX line profile (B) and X-ray mapping (C and D).

obtained nanostructures crystallize according the Cu_7Te_4 phase (SG: $P\bar{3}m1$) (JCPDS n°04-024-0587) (Fig. 6). These results corroborate the XRD analyses (Fig. 3). From a crystallographic point of view, this chemical transformation from Te to Cu_7Te_4 is made easier since the atomic arrangement of tellurium is preserved from one phase to another. Indeed, Cu_7Te_4 is composed of a distorted hexagonal sublattice of tellurium atoms, with the copper atoms being located between these layers.

SEM investigations (Fig. 4) devoted to the morphology point out that Cu_7Te_4 particles have a hexagonal prismatic shape dictated by the symmetry elements of its point group $\bar{3}m$ [39,40]. This observation is a consequence of a transformation in a liquid solution, considered as an isotropic medium. The hexagonal prismatic shape is an open form [41] having, at least, one additional form in order to completely enclose the space surrounding the matter. From the energetic point of view, this shape, dictated by the $\bar{3}m$ point group, corresponds to an absolute extremum [42], an indicator of the stability of this copper telluride.

The distribution of the copper and tellurium atoms in the unit cell is illustrated in 3D by Fig. 7A [38]. Based on this organization, the copper telluride can be described by a stacking of 3 different parallel layers, namely A, M and B along the [001] direction (Fig. 7B). It can be notice that the layers A and B are composed by 4 Cu and 4 Te while the M layer is exclusively formed by 6 Cu atoms. Fig. 7C represents the high-angle annular dark field (HAADF) micrograph recorded along [010] direction of the Cu_7Te_4 lattice with the superimposition of the simulated crystal structure in the same direction. The three extended layers A, M and B mentioned above are parallel to the crystallographic plane (001). Attention has to be attracted by the breaking of the stacking atomic layers leading to stacking fault (Fig. 7C). A profile plot (Fig. 7D) along a line-segment shows the atomic distribution and points out the stacking defects.

In addition, the presence of these stacking faults results diffusion intensity lines (DIL) on the FFT (Fig. 6 inset) recorded along [010] zone axis. Fig. 8 reinforces the hypothesis of the single crystallinity of the transformed nanostructures of copper telluride with similar SAED and FFT patterns. Moreover, some nanorods appear curved as shown in the HRTEM micrographs (Fig. 8A). Similar phenomenon has also been observed by other authors [3]. This observation could be the consequence of the presence of local defects, as suggested by the presence of diffuse diffracted lines instead of spots in Fig. 8B. Growth steps (kinks) are observed on the edges of Cu_7Te_4 nanorods (Fig. 8B), which are associated to ledge mechanism (terraces and front). The stacking defects could generate stress and their density would cause plane shifts since the defect faults are oriented in the same direction. Then the deviation from the hexagonal prismatic shape could be explained by the presence of planar defects. Another explanation for this curvature could be the crystalline symmetry of the hexagonal phase that imposes this geometry on the nanostructures. However, this second hypothesis is rather

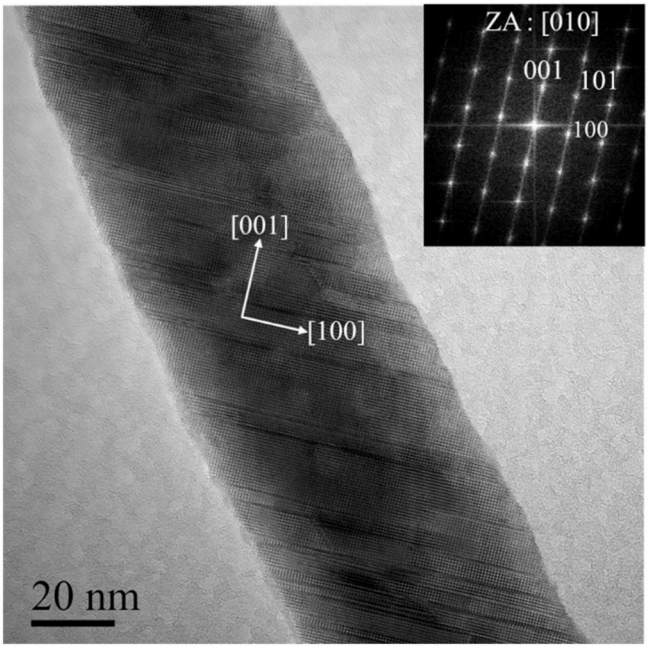

Fig. 6. HRTEM micrograph of copper telluride nanorods after 2 h of reaction in bath B (Cu large excess/$C_6H_8O_6$ stoichiometry) and zooming on the crystallographic structure of Cu_7Te_4 along the [010] zone axis with FFT (SG: $P\bar{3}m1$ (164) (JCPDS: #04-024-0587).

unlikely, since all nanorods are not curved. The local atomic defects are probably due to the rapid redox reaction involved in the conversion of Te to Cu_7Te_4 by opposition to a slow topotactic reaction mechanism [14,23]. Indeed, topotactic conversion is a quite slow process that leads usually to structures with no local defaults [27].

The oxidation state of copper was first studied by EELS (Fig. 9). The fine structures of the ionization thresholds based on the electronic transitions were determined and compared with standards Cu_2O, CuO and Cu. In the case of copper, the first L3 peak corresponds to the $2p_{3/2} \rightarrow 3d_{3/2}$ or $2p_{3/2} \rightarrow 3d_{5/2}$ transitions, whereas the second L2 corresponds to the $2p_{1/2} \rightarrow 3d_{3/2}$ transition. The shape of the spectrum is qualitatively similar to that of Cu_2O. Moreover, the intensity ratio L3/L2 of Cu_7Te_4 is close to that of Cu_2O. As a result, this analysis suggests the copper to be present in major proportion at its oxidation state of +I. This result is in line with the literature in which most experimental characterizations, obtained mainly by X-ray photoelectron spectroscopy, show the presence of Cu(I) and Te(-II) in Cu_7Te_4 nanostructures [4,43,44]. Only the recent study by Li et al. [6] suggests mixed valences of Cu in nanosheets of Cu_7Te_4 prepared by vacuum solid-liquid reaction, namely Cu^0, Cu(I) and Cu(II).

To further confirm the chemical environment of Cu, XPS analysis has been performed on Cu_7Te_4 nanorods (Fig. 10). The Cu signal exhibit a doublet centered at 932.5 eV and with a very weak satellite around 945 eV. This is a typical signature of Cu(I), as Cu(II) should exhibit a strong satellite peak [45]. The signal of Te is more complex, as it also includes the Cu LMM Auger peak. Therefore, a proper fitting is not possible due to this overlap and the complexity of finding the right background. First, the Te peak exhibit a clear doublet, with Te $3d_{5/2}$ centered at 572.9 eV, attributed to Te(-II) [46,47]. Slight oxidation of the Te is observed with the presence of a Te $3d_{5/2}$ doublet centered at 575.6 eV. The Cu LMM contribution is composed of several peaks. First, a wide peak at 569.4 eV is present, with a superimposed sharp peak at around 568.3 eV. These attribution are attributed to Auger peak of Cu(I) and Cu(II) respectively, in agreement with Biesinger [48] and Platzman et al. [49].

Therefore, XPS confirms EELS analysis, with Cu predominantly in (+I) oxidation state, and the presence of (+II) oxidation state visible on Auger peak.

The influence of the n(Cu(II))/n(Te) ratio was also studied, keeping n($C_6H_8O_6$)/n(Cu(II)) = 0.5. For this purpose, n(Cu(II))/n(Te) varied between 772 down to 2 (baths B to D). The XRD analysis of the samples was used as an indicator of Te conversion. According to the analysis of the diffraction patterns, only a very large excess of Cu(II) over Te (n(Cu(II))/n(Te) = 772) leads to a total Te transformation after 2 h immersion (Fig. 11). Indeed, this is the only studied ratio for which the peaks corresponding to Te at 27.7, 49.8 and 57.1° disappear completely and the peaks corresponding to Cu_7Te_4 appear at 24.6 and 27.5°. The XRD analysis is confirmed by TEM analysis of individual nanorods for the n(Cu(II))/n(Te) = 400 ratio (bath C), the nanorods are single-crystalline and the electron diffraction pattern is indexed according the initial hexagonal Te phase (See supporting information: Figure SI-1). Moreover, the atomic percentage of copper measured by ICP-OES after dissolution of nanorods obtained with n(Cu(II))/n(Te) = 400 is equal to 11%, highlighting that there is only a partial conversion of Te nanorods. These results suggest that a large ratio n(Cu(II))/n(Te) is necessary for a complete conversion of Te into copper telluride. This is not in agreement with the work of Zhou et al. who obtain a complete conversion for n(Cu(II))/n(Te) = 2 and n($C_6H_8O_6$)/n(Cu(II)) = 0.5 in ethylene glycol. However, in their work, these authors underline the importance of the order of introduction of the reactants in the reaction medium. Indeed, Zhou et al. add ascorbic acid after mixing Te and Cu(II) solutions in order to promote the reaction at the surface of Te by adsorption of Cu(II) [13]. Therefore, we performed a conversion test by adding ascorbic acid 15 min after introducing the Te deposit into the Cu(II) solution. However, the conversion of Te was still not complete even after 24 h. The same observations were obtained by increasing the n($C_6H_8O_6$)/n(Cu(II)) ratio to 2. The main difference with the work of Zhou et al. and this project is the use ethylene glycol, that can also act as a reducing agent like $C_6H_8O_6$ [13].

Finally, the influence of the duration of Te immersion on its conversion was studied, using the optimal experimental conditions defined above, namely n(Cu(II))/n(Te) = 772 and n($C_6H_8O_6$)/n(Cu(II)) = 0.5 (Bath B). XRD analysis revealed that the Te peaks already disappear after 15 min of impregnation, confirming that the conversion reaction of Te is a fast reaction. TEM-EDX analysis confirms that Te nanorods are converted to Cu_7Te_4 after 15 min. By TEM crystallographic analysis, the previous discussions are confirmed with the indexing of single crystal nanostructures to the phase Cu_7Te_4 and the presence of stacking defects.

These experimental results show a rapid transformation to Cu_7Te_4, which requires a large ratio n(Cu(II))/n(Te). We can thus hypothesize a dismutation-type redox reaction. We have attempted to validate this hypothesis using the following thermodynamic approach.

3.1. Thermodynamic considerations

There is very little literature data regarding the oxidation states of Cu and Te in copper telluride compounds but a few XPS results can be found: Zhang et al. detected the presence of Cu(I) and Te(-II) in Cu_2Te [50], whereas Cu(II) and Te(-II) were identified in CuTe by She et al. [26]. In between these two defined compounds, non-stoichiometric copper telluride $Cu_{2-x}Te$ can exist in a wide range of compositions and phases. According to Pashinkin et al. [51], all of the crystal phases in the Cu–Te system consist of a rigid Te framework and mobile Cu ions in different valence states, Cu(I) or Cu(II), with the arrangement of the Cu ions depending on the composition. The EELS and XPS characterization of Cu_7Te_4 nanostructures synthesized in our work revealed that copper is mainly present as Cu(I) with minor presence of Cu(II). Therefore, in line with the results of EELS and XPS chemical analyses, and also according to above cited literature, we assume a combination of 1 Cu(II) and 6 Cu(I) along with 4 Te(-II) in Cu_7Te_4 to ensure the charge balance.

The hypothesis of a chemical conversion of Te(0) into copper telluride involving a disproportionation reaction of Te(0), as assumed by Park et al. [24], seems the most likely. This is also supported by the fact that the reaction of conversion is quite fast, by opposition to a topotactic

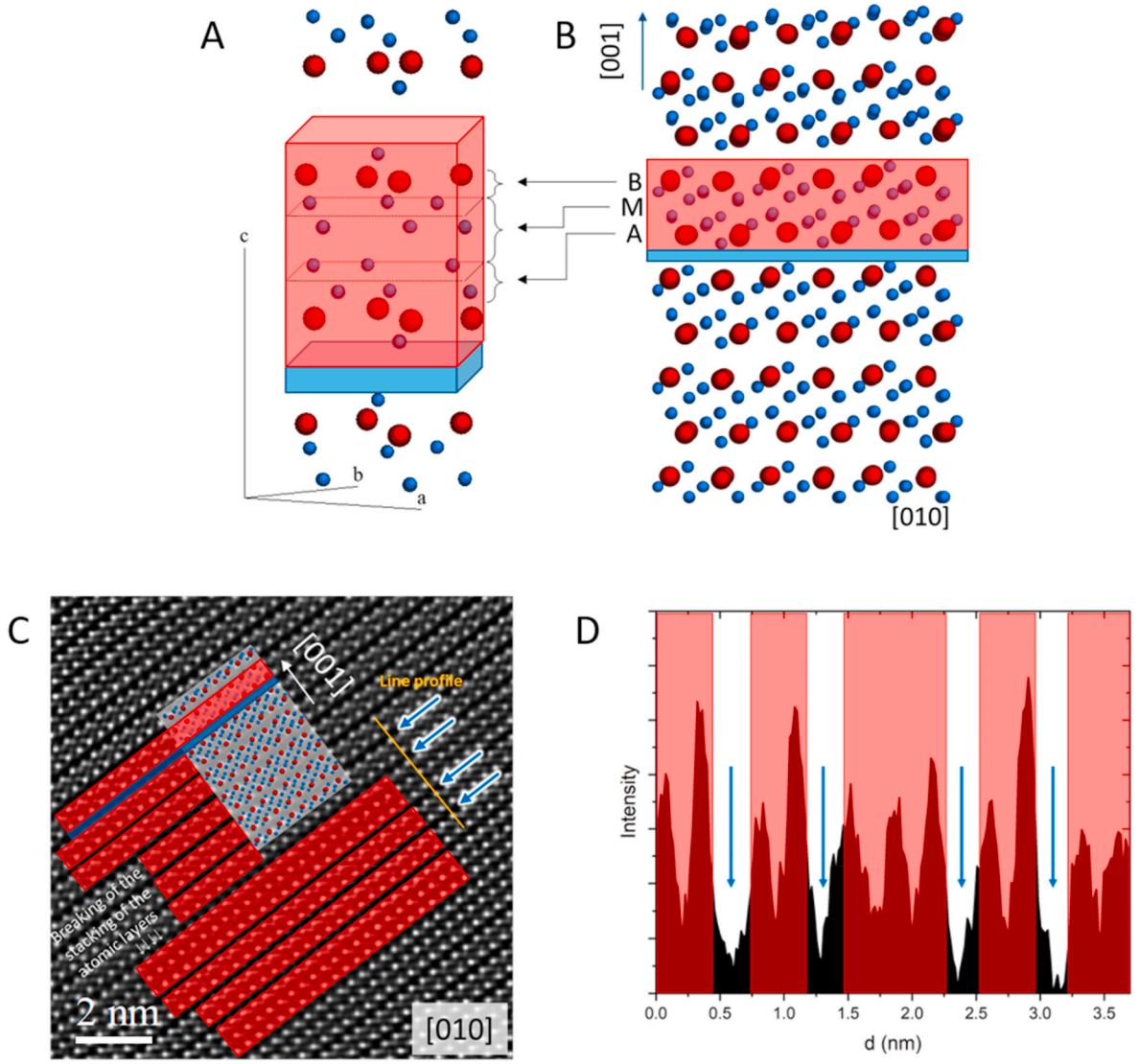

Fig. 7. Schematic representation of the Cu_7Te_4 crystal lattice with copper and tellurium atoms in blue and red, respectively, in 3D view [38] (A) and along the [010] zone axis (B). TEM characterizations of copper telluride nanorods after 2 h of reaction in bath B: High-angle annular dark-field (HAADF) imaging by STEM with Cu_7Te_4 lattice superimposed (C) and line profile analysis showing stacking defect (D). (For interpretation of the references to colour in this figure legend, the reader is referred to the Web version of this article.)

reaction as proposed by other authors [14,23].

We propose then the following mechanism:

– The formation of Cu(I) by *in situ* reduction of Cu(II) ions by ascorbic acid (Eq. (2)) induces Te(0) disproportionation reaction into Te(-II) and Te(IV) (Eq. (5)), leading instantaneously to Cu_7Te_4 formation (Eq. (6)).

$$3Te(0) \rightarrow Te(IV) + 2\,Te(-II) \quad \text{Eq. 5}$$

$$Cu(II) + 6\,Cu(I) + 4\,Te(-II) \rightarrow Cu_7Te_4 \quad \text{Eq. 6}$$

This can be globally written as Eq. (7):

$$Cu(II) + 6\,Cu(I) + 4\,Te(0) + 8\,e^- \rightarrow Cu_7Te_4\ ;\ \Delta_r G^0_{Cu(II),Cu(I),Te(0)/Cu_7Te_4} \quad \text{Eq. 7}$$

The pH value of the aqueous solution used in this work for the conversion of Te nanorods is equal to 3.2, consequently, the predominant dissolved species are Cu^{2+} for Cu(II) and $HTeO_2^+$ for Te(IV). The overall equation of the conversion reaction, including Cu^{2+} reduction by ascorbic acid, can then be written as (Eq. (8)):

$$6\,Te(0) + 7\,Cu^{2+} + 3\,C_6H_8O_6 + 4\,H_2O \rightarrow 2\,HTeO_2^+ + Cu_7Te_4 + 3\,C_6H_6O_6 + 12\,H^+ \quad \text{Eq. 8}$$

The disproportionation reaction of Te(0) is supported by thermodynamic considerations, by comparing the formal redox potential values E^0 of $HTeO_2^+$/Te(0) and Cu(II), Cu(I), Te(0)/Cu_7Te_4. The latter can be calculated as follow. Eq. (7) can be considered as a linear combination of Eq. (9) to Eq. (11):

$$7\,Cu(0) + 4\,Te(0) \rightleftarrows Cu_7Te_4\ ;\ \Delta_f G^0_{Cu_7Te_4} \quad \text{Eq. 9}$$

$$Cu(I) + e^- \rightleftarrows Cu(0)\ ;\ \Delta_{1/2} G^0_{Cu(I)/Cu(0)} \quad \text{Eq. 10}$$

$$Cu(II) + 2\,e^- \rightleftarrows Cu(0)\ ;\ \Delta_{1/2} G^0_{Cu(II)/Cu(0)} \quad \text{Eq. 11}$$

where $\Delta_X G^0_i$ is the Gibbs free energy related to the associated reactions.

– According to the Hess law, the following relation can be written (Eq. (12)):

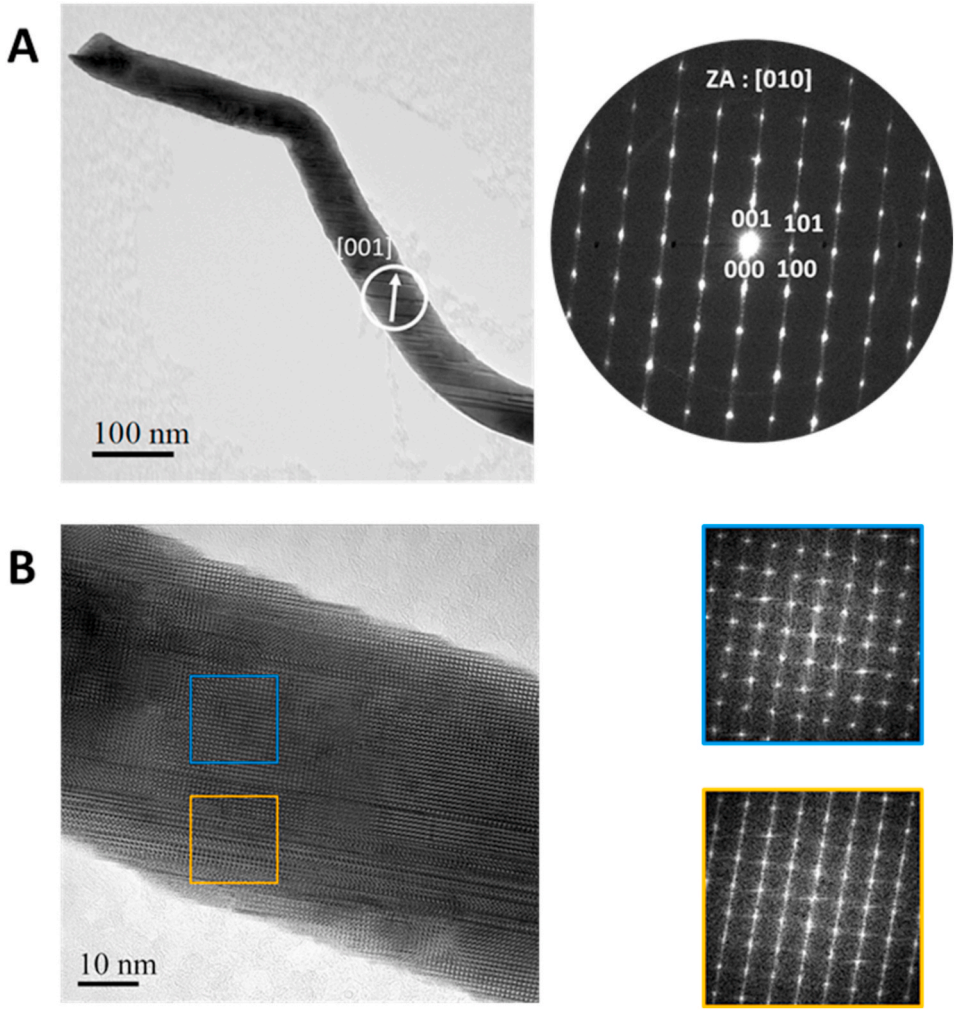

Fig. 8. TEM characterizations of copper telluride nanorods after 2 h of reaction in bath B (Cu large excess/$C_6H_8O_6$ stoichiometry). A) HRTEM and SAED analysis (zone axis [010]) B) HRTEM zoom on growth steps along the nanorods and FFT showing stacking defect (orange) and no defect (blue). (For interpretation of the references to colour in this figure legend, the reader is referred to the Web version of this article.)

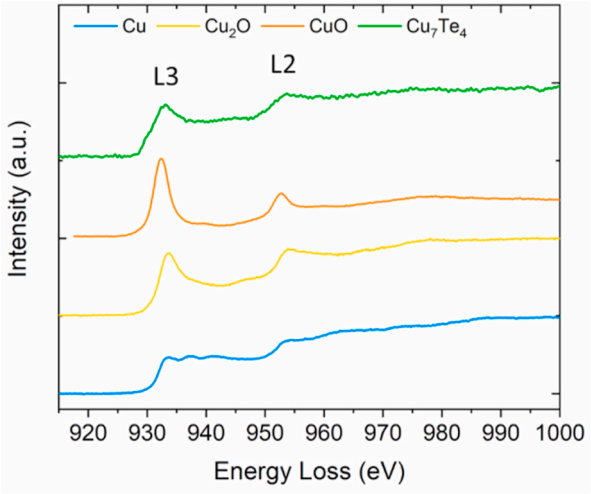

Fig. 9. EELS characterization of Cu_7Te_4 nanorods (in green) by comparison with different standards of copper at different oxidation states (Cu in blue, Cu_2O in yellow and CuO in orange). (For interpretation of the references to colour in this figure legend, the reader is referred to the Web version of this article.)

$$\Delta_r G^0_{Cu(II),Cu(I),Te(0)/Cu_7Te_4} = \Delta_f G^0_{Cu_7Te_4} + 6 \times \Delta_{1/2} G^0_{Cu(I)/Cu(0)} + \Delta_{1/2} G^0_{Cu(II)/Cu(0)} \quad \text{Eq. 12}$$

Then, the formal redox potential of Cu(II), Cu(I), Te(0)/Cu_7Te_4 can be calculated according the following equation (Eq. 13):

$$-8.\mathcal{F} E^0_{Cu(II),Cu(I),Te/Cu_7Te_4} = \Delta_f G^0_{Cu_7Te_4} - 6.\mathcal{F} E^0_{Cu(I)/Cu} - 2.\mathcal{F} E^0_{Cu(II)/Cu} \quad \text{Eq. 13}$$

The value of the Gibbs free energy of formation of Cu_7Te_4, $\Delta_f G^0_{Cu_7Te_4}$, can be found in the literature ($\Delta_f G^0_{Cu_{7+x}Te_4} = -170,30$ kJ·mol^{-1} [52]). In the experimental conditions of this work, we assume that the dissolved cations Cu(II) in the baths are not chelated and are present under the form Cu^{2+}, with $E^0_{Cu^{2+}/Cu} = 0.34$ V vs SHE. With respect to Cu(I), we consider the related potential $E^0_{Cu^{+}/Cu} = 0.52$ V vs SHE. So, the potential of the redox couple Cu^{2+}, Cu^{+}, Te/Cu_7Te_4 is then calculated at 0,70 V vs SHE. By considering at pH = 3.2 the formal redox potential of $HTeO_2^+$/Te(0) $E^0_{HTeO_2^+/Te(0)} = 0,41$ V vs SHE [53], $E^0_{Cu^{2+},Cu^{+},Te(0)/Cu_7Te_4}$ is then superior to $E^0_{HTeO_2^+/Te(0)}$ meaning that the mechanism based on Te(0) disproportionation reaction is thermodynamically favorable.

4. Conclusion

Cu_7Te_4 single-crystalline nanorods were successfully synthesized by a two-step synthesis route. First, nanorods of tellurium were obtained by

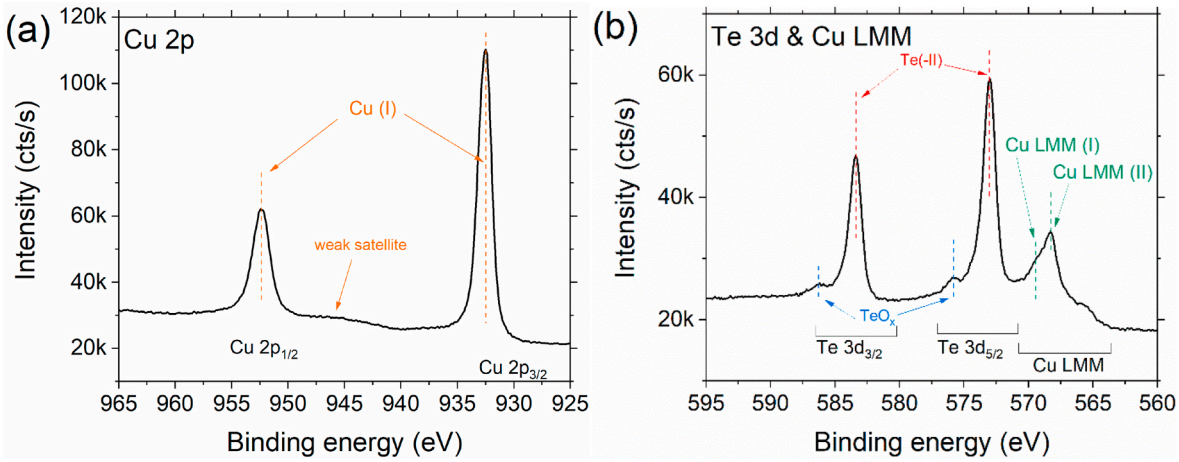

Fig. 10. XPS analysis of Cu_7Te_4 nanorods: Cu 2p and Te 3d XPS levels (including Cu LMM Auger peaks).

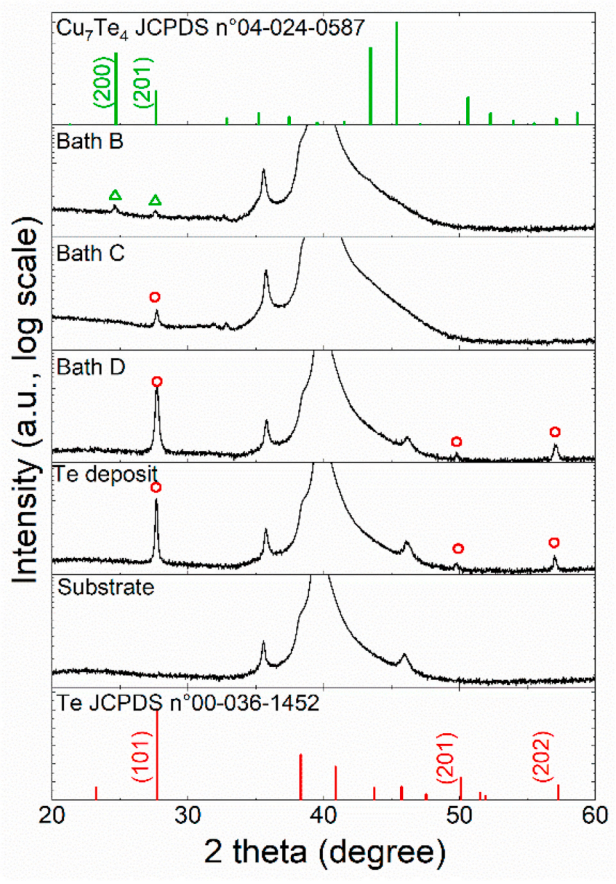

Fig. 11. XRD characterizations to study the influence of molar ratio Cu(II)/Te after 2 h immersion in bath B (Cu large excess/$C_6H_8O_6$ stoichiometry), in bath C (Cu excess/$C_6H_8O_6$ stoichiometry) and in bath D (Cu near stoichiometry/$C_6H_8O_6$ stoichiometry) on the crystallographic transition from Trigonal Te to trigonal Cu_7Te_4, using, for convenience, hexagonal unit cells.

electrochemical deposition in an ionic liquid electrolyte. Then, they were converted into Cu_7Te_4 by Te(0) disproportionation in the presence of Cu(I), induced by initial reduction of Cu(II) precursor with ascorbic acid. This mechanism is supported by EELS analysis that highlights the major presence of Cu(I) into the converted phase, and by thermodynamics considerations. Different experimental parameters of the chemical step were studied namely, Cu(II):Te and Cu(II):$C_6H_8O_6$ molar ratios and the conversion reaction time. It has been demonstrated that ascorbic acid should be introduced in stoichiometric proportion regarding Cu(II) in order to avoid the formation of Cu(0) at the surface of the film of nanorods. Then, Cu(II) has to be added in large excess regarding tellurium nanorods and it appears that 15 min was enough to already have the full conversion of tellurium into Cu_7Te_4. Moreover, these materials exhibit a homogenous chemical composition and a single crystallinity. The presence of stacking local defects is highlighted, leading to curved nanostructures. Finally, the crystalline quality of the final nanostructures standing on the electrodes could present interesting thermal and electronic properties for energy applications.

CRediT authorship contribution statement

K. Al Hokayem: Conceptualization, Methodology, Writing – original draft. **L.M. Adam:** Methodology, Visualization, Writing – review & editing. **J. Ghanbaja:** Methodology. **A. Redjaïmia:** Methodology. **E. Haye:** Methodology. **S. Michel:** Methodology. **S. Legeai:** Conceptualization, Validation, Writing – review & editing. **N. Stein:** Conceptualization, Validation, Visualization, Writing – review & editing.

Declaration of competing interest

The authors declare that they have no known competing financial interests or personal relationships that could have appeared to influence the work reported in this paper.

Data availability

Raw data corresponding to this research work are available in open access at: https://doi.org/10.12763/QEGAXU.

Acknowledgements

This work was supported by the Grand Est Region under the Nanohyb project. SIAM platform from UNamur is acknowledged for XPS measurements.

Appendix A. Supplementary data

Supplementary data to this article can be found online at https://doi.org/10.1016/j.matchemphys.2024.129239.

References

[1] C. Coughlan, M. Ibanez, O. Dobrozhan, A. Singh, A. Cabot, K.M. Ryan, Compound copper chalcogenide nanocrystals, Chem. Rev. 117 (2017) 5865–6109.

[2] B. Mansour, B. Farag, S. Khodier, Transport properties and band structure of non-stoichiometric $Cu_{2-x}Te$, Thin Solid Films 247 (1994) 112–119.

[3] L.P. Tan, T. Sun, S. Fan, L.Y. Ng, A. Suwardi, Q. Yan, H.H. Hng, Facile synthesis of Cu_7Te_4 nanorods and the enhanced thermoelectric properties of Cu_7Te_4–$Bi_{0.4}Sb_{1.6}Te_3$ nanocomposites, Nano Energy 2 (2013) 4–11.

[4] C. Nethravathi, C.R. Rajamathi, M. Rajamathi, R. Maki, T. Mori, D. Golberg, Y. Bando, Synthesis and thermoelectric behaviour of copper telluride nanosheets, J. Mater. Chem. A 2 (2014) 985–990.

[5] W. Li, Y. Ma, P. Li, X. Jing, K. Jiang, D. Wang, Electrochemically activated $Cu_{2-x}Te$ as an Ultraflat discharge plateau, low reaction potential, and stable anode material for aqueous Zn-ion half and full batteries, Adv. Energy Mater. 11 (2021) 2102607.

[6] W. Li, Y. Ma, H. Shi, K. Jiang, D. Wang, Cu_7Te_4 as an anode material and Zn dendrite inhibitor for aqueous Zn-ion battery, Adv. Funct. Mater. 32 (2022) 2205602.

[7] Q. Qin, G. Zhang, Z. Chai, J. Zhang, Y. Cui, T. Li, W. Zheng, Ionic liquid-assisted synthesis of Cu_7Te_4 ultrathin nanosheets with enhanced electrocatalytic activity for water oxidation, Nano Energy 41 (2017) 780–787.

[8] F. Golgovici, A.-S. Catrangiu, T. Visan, The Formation and characterization of copper telluride films from choline chloride–urea ionic liquid, Int. J. Electrochem. Sci. 11 (2016) 915–928.

[9] M. Huang, A. Maljusch, F. Calle-Vallejo, J.B. Henry, M.T. Koper, W. Schuhmann, A. S. Bandarenka, Electrochemical formation and surface characterisation of $Cu_{2-x}Te$ thin films with adjustable content of Cu, RSC Adv. 3 (2013) 21648–21654.

[10] E. Rudnik, J. Kozłowski, Electrochemical studies on the codeposition of copper and tellurium from acidic nitrate solution, Electrochim. Acta 107 (2013) 103–110.

[11] S. Arya, S. Khan, S. Kumar, R. Verma, P. Lehana, Synthesis of copper telluride nanowires using template-based electrodeposition method as chemical sensor, Bull. Mater. Sci. 36 (2013) 535–539.

[12] Z.Y. Aydın, S. Abacı, Characterization of CuTe nanofilms grown by underpotential deposition based on an electrochemical codeposition technique, J. Solid State Electrochem. 21 (2017) 1417–1430.

[13] C. Zhou, C. Dun, Q. Wang, K. Wang, Z. Shi, D.L. Carroll, G. Liu, G. Qiao, Nanowires as building blocks to fabricate flexible thermoelectric fabric: the case of copper telluride nanowires, ACS Appl. Mater. Interfaces 7 (2015) 21015–21020.

[14] G.-H. Dong, Y.-J. Zhu, G.-F. Cheng, Y.-J. Ruan, Cu(2−X)Te nanowires synthesized by a microwave-assisted solvothermal method using a self-sacrificial template and their electrical conductivity, Mater. Lett. 76 (2012) 69–72.

[15] C. Han, Z. Li, W.-j. Li, S.-l. Chou, S.-x. Dou, Controlled synthesis of copper telluride nanostructures for long-cycling anodes in lithium ion batteries, J. Mater. Chem. A 2 (2014) 11683–11690.

[16] Q. Wang, G. Chen, X. Shi, R. Jin, L. Wang, D. Chen, Controllable synthesis of Cu_7Te_4 nanoparticles and sheet-like particles through the delayed reaction and their thermal stability, Powder Technol. 207 (2011) 192–198.

[17] B. Li, Y. Xie, J. Huang, H. Su, Y. Qian, A solvothermal route to nanocrystalline Cu_7Te_4 at low temperature, J. Solid State Chem. 146 (1999) 47–50.

[18] B. Li, Y. Xie, J. Huang, Y. Liu, Y. Qian, Sonochemical synthesis of nanocrystalline copper tellurides Cu_7Te_4 and Cu_4Te_3 at room temperature, Chem. Mater. 12 (2000) 2614–2616.

[19] C.-C. Lin, W.-F. Lee, M.-Y. Lu, S.-Y. Chen, M.-H. Hung, T.-C. Chan, H.-W. Tsai, Y.-L. Chueh, L.-J. Chen, Low temperature synthesis of copper telluride nanostructures: phase formation, growth, and electrical transport properties, J. Mater. Chem. 22 (2012) 7098–7103.

[20] B. Wan, C. Hu, W. Zhou, H. Liu, Y. Zhang, Construction of strong alkaline hydrothermal environment for synthesis of copper telluride nanowires, Solid State Sci. 13 (2011) 1858–1864.

[21] P. Kumar, K. Singh, Element directed aqueous solution synthesis of copper telluride nanoparticles, characterization, and optical properties, Cryst. Growth Des. 9 (2009) 3089–3094.

[22] I. Kriegel, C. Jiang, J. Rodríguez-Fernández, R.D. Schaller, D.V. Talapin, E. Da Como, J. Feldmann, Tuning the excitonic and plasmonic properties of copper chalcogenide nanocrystals, J. Am. Chem. Soc. 134 (2012) 1583–1590.

[23] H. Wang, P. Zuo, A. Wang, S. Zhang, C. Mao, J. Song, H. Niu, B. Jin, Y. Tian, Facile synthesis and electrochemical property of Cu_2Te nanorods, J. Alloys Compd. 581 (2013) 816–820.

[24] D. Park, H. Ju, T. Oh, J. Kim, Facile fabrication of one-dimensional Te/Cu_2Te nanorod composites with improved thermoelectric power factor and low thermal conductivity, Sci. Rep. 8 (2018) 18082.

[25] S. Kumar, V. Singh, A. Vohra, S. Chakarvarti, Morphology and optical properties of template synthesized copper-telluride nanowires, Am. J. Mater. Sci. Technol. 1 (2013) 74–85.

[26] G. She, X. Zhang, W. Shi, Y. Cai, N. Wang, P. Liu, D. Chen, Template-free electrochemical synthesis of single-crystal CuTe nanoribbons, Cryst. Growth Des. 8 (2008) 1789–1791.

[27] K. Al Hokayem, J. Ghanbaja, S. Michel, S. Legeai, N. Stein, Insights in the two-step synthesis of single crystalline Ag_2Te nanorods, Mater. Chem. Phys. 289 (2022) 126487.

[28] Y. Traore, S. Legeai, S. Diliberto, G. Arrachart, S. Pellet-Rostaing, M. Draye, New insight into indium electrochemistry in a Tf_2N-based room-temperature ionic liquid, Electrochim. Acta 58 (2011) 532–540.

[29] J. Szymczak, S. Legeai, S. Diliberto, S. Migot, N. Stein, C. Boulanger, G. Chatel, M. Draye, Template-free electrodeposition of tellurium nanostructures in a room-temperature ionic liquid, Electrochem. Commun. 24 (2012) 57–60.

[30] L. Thiebaud, S. Legeai, N. Stein, Tuning the morphology of Te one-dimensional nanostructures by template-free electrochemical deposition in an ionic liquid, Electrochim. Acta 197 (2016) 300–306.

[31] L. Thiebaud, S. Legeai, J. Ghanbaja, N. Stein, Electrodeposition of high aspect ratio single crystalline tellurium nanowires from piperidinium-based ionic liquid, Electrochim. Acta 222 (2016) 528–534.

[32] N. Kumar, R. Kumar, S. Kumar, S.K. Chakarvarti, Optical and electrical studies of vertically oriented tellurium nanowire arrays produced by template electrodeposition, J. Electron. Mater. 44 (2015) 2939–2945.

[33] L. Thiebaud, S. Legeai, J. Ghanbaja, N. Stein, Synthesis of Te-Bi core-shell nanowires by two-step electrodeposition in ionic liquids, Electrochem. Commun. 86 (2018) 30–33.

[34] G. Greczynski, L. Hultman, Compromising science by ignorant instrument calibration—need to revisit half a century of published XPS data, Angew. Chem. Int. Ed. 59 (2020) 5002–5006.

[35] G. Greczynski, L. Hultman, X-ray photoelectron spectroscopy: towards reliable binding energy referencing, Prog. Mater. Sci. 107 (2020) 100591.

[36] J.W. Pinder, G.H. Major, D.R. Baer, J. Terry, J.E. Whitten, J. Čechal, J.D. Crossman, A.J. Lizarbe, S. Jafari, C.D. Easton, J. Baltrusaitis, M.A. van Spronsen, M.R. Linford, Avoiding common errors in X-ray photoelectron spectroscopy data collection and analysis, and properly reporting instrument parameters, Appl. Surface Sci. Adv. 19 (2024) 100534.

[37] X. Guo, T. Zhang, J. Li, T. Fan, Butterfly-scale architecture directed electrodeposition of Ag microband arrays for electrochemical detection, RSC Adv. 4 (2014) 59508–59512.

[38] P. Koch, S. Steinberg, Exploring the subtle factors that control the structural preferences in Cu_7Te_4, J. Phys. Condens. Matter 35 (2023) 064003.

[39] M. Buerger, Elementary Crystallography: an Introduction to the Fundamental Geometrical Features of Crystals, second ed., The MIT Press, 1978.

[40] H. Kabbara, J. Ghanbaja, A. Redjaïmia, T. Belmonte, Crystal structure, morphology and formation mechanism of a novel polymorph of lead dioxide, γ-PbO_2, J. Appl. Crystallogr. 52 (2019) 304–311.

[41] F.C. Phillips, Introduction to Crystallography, John Wiley & Sons Canada, Limited, 1971.

[42] J. Cahn, G. Kalonji, H. Aaronson, D. Laughlin, R. Sekerka, C. Wayman, Solid-solid Phase Transformations, TMS-AIME, 1982, pp. 3–14. Aaronson, H. I., Sekereka, R. F., Laughlin, D. E., Waymann, C.M. , Warrendale, PA.

[43] S. Liu, W. Xia, K. Huang, D. Pei, T. Deng, A. Liang, J. Jiang, H. Yang, J. Zhang, H. Zheng, Measurement of electronic structure and surface reconstruction in the superionic $Cu_{2-x}Te$, Phys. Rev. B 103 (2021) 115127.

[44] S. Harish, T. Saha, S. Kavirajan, M. Omprakash, E. Senthil Kumar, M. Navaneethan, Bismuth induced Cu_7Te_4/Sb_2Te_3 nanocomposites for higher thermoelectric power factor and carrier properties, J. Mater. Sci. Mater. Electron. 33 (2022) 8804–8814.

[45] M.C. Biesinger, L.W.M. Lau, A.R. Gerson, R.S.C. Smart, Resolving surface chemical states in XPS analysis of first row transition metals, oxides and hydroxides: Sc, Ti, V, Cu and Zn, Appl. Surf. Sci. 257 (2010) 887–898.

[46] C. Wagner, A. Naumkin, A. Kraut-Vass, J. Allison, C. Powell, J. Rumble Jr., NIST Standard Reference Database 20, National Institute of Standards and Technology, Gaithersburg, MD, 2003 20899 (Web version), Version 3.4.

[47] J.F. Moulder, W. Stickle, P. Sobol, K. Bomben, Handbook of X-Ray Photoelectron Spectroscopy, 1992, p. 1992.

[48] M.C. Biesinger, Advanced analysis of copper X-ray photoelectron spectra, Surf. Interface Anal. 49 (2017) 1325–1334.

[49] I. Platzman, R. Brener, H. Haick, R. Tannenbaum, Oxidation of polycrystalline copper thin films at ambient conditions, J. Phys. Chem. C 112 (2008) 1101–1108.

[50] Y. Zhang, Z.-P. Qiao, X.-M. Chen, Microwave-assisted elemental direct reaction route to nanocrystalline copper chalcogenides CuSe and Cu_2Te, J. Mater. Chem. 12 (2002) 2747–2748.

[51] A. Pashinkin, V. Fedorov, Phase equilibria in the Cu–Te system, Inorg. Mater. 39 (2003) 539–554.

[52] A. Pashinkin, L. Pavlova, Standard functions of formation and thermodynamic stability of compounds in the Cu-Te system, Inorg. Mater. 41 (2005) 1050–1054.

[53] M. Pourbaix, Atlas D'équilibres Électrochimiques, Gauthier-Villars and C'Editeur Paris, 1963.